Characterization of the vortex-pair interaction law and nonlinear mobility effects

2013 New J. Phys. 15 013028

(http://iopscience.iop.org/1367-2630/15/1/013028)

New Journal of Physics
The open access journal for physics

Characterization of the vortex-pair interaction law and nonlinear mobility effects

R Barboza[1,2,4], T Sauma[1,3], U Bortolozzo[1], G Assanto[2], M G Clerc[3] and S Residori[1]

[1] INLN, Université de Nice-Sophia Antipolis, CNRS, 1361 Route des Lucioles, F-06560 Valbonne, France
[2] NooEL-Nonlinear Optics and OptoElectronics Lab., University Roma Tre, Via della Vasca Navale 84, I-00146 Rome, Italy
[3] Departamento de Física, FCFM, Universidad de Chile, Casilla 487-3, Santiago, Chile
E-mail: raouf.barboza@inln.cnrs.fr, umberto.bortolozzo@inln.cnrs.fr, assanto@uniroma3.it, marcel@dfi.uchile.cl and stefania.residori@inln.cnrs.fr

New Journal of Physics **15** (2013) 013028 (9pp)
Received 3 October 2012
Published 15 January 2013
Online at http://www.njp.org/
doi:10.1088/1367-2630/15/1/013028

Abstract. Employing nematic liquid crystals in a homeotropic cell with a photosensitive wall, dissipative vortex pairs are selectively induced by external illumination and the interaction law is characterized for pairs of opposite topological charges. Contrary to the phenomenological fit with a force inversely proportional to the distance, the data provide evidence that nonlinear mobility effects must be taken into account. The observations lead to a reconciliation of experiments with theory.

[4] Author to whom any correspondence should be addressed.

Contents

Out of equilibrium systems exhibit instabilities leading to spontaneous symmetry breaking and pattern formation [1]. Owing to fluctuations, different organizations may emerge in distinct regions of the same sample; hence, spatial structures are usually characterized by domains, separated by interfaces, such as grain boundaries, defects or dislocations [2]. Among others, defects in rotationally invariant systems, i.e. vortices, attract a great deal of attention because of their universal character, as they are solutions of the complex Ginzburg–Landau equation (CGLE) that describes such different systems as fluids, superfluids, superconductors, liquid crystals, magnetic media and optical dielectrics [3]. Vortices occur in complex fields and can be identified as topological defects, that is, point-like singularities which locally break the symmetry [4]. They exhibit zero intensity at the singular point with a phase spiraling around it: the topological charge is assigned by counting the number of spiral arms in the phase distribution, while the sign is given by the sense of the spiral rotation. In optics, the latter procedure is equivalent to counting the number of extra or missing fringes in the dislocation of an interference pattern [5].

Optical vortices have recently generated substantial interest in their applications, from optical tweezers [6, 7], to quantum computation [8], enhanced astronomical imaging [9] and high-contrast coronagraph for exoplanet detection [10]. The implementation of suitable defects in soft matter is considered as one of the most efficient ways of generating vortices via exchange of angular momentum between light and matter [11, 12]. In liquid crystals, vortices can be generated by applying electric or magnetic fields [13] and appear as self-assembling topological defects, well described by the CGLE [14]. Their behavior is ruled by a dissipative dynamics and is characterized by a coarsening process [15]. If this dynamics could be controlled, defects in liquid crystal textures could be employed, for instance, in light manipulation [16] or to fabricate self-assembled metamaterials [17], photonic crystals and bio-sensors via colloidal structures [18].

In general, vortices lack an analytical expression and are described by a Padé approximation [2, 3]. As for the interaction law between dissipative vortex pairs, a discrepancy between the theoretical and the phenomenological description remains open. Indeed, the phenomenological description is based on a constant vortex mobility, leading to a force inversely proportional to the distance, in contrast with the theory that accounts for a nonlinear mobility. The first experimental results of Nagaya *et al* [19] were interlocutory and were in contrast with the effective dynamics derived from the Frank energy formalism in nematics [13]. Later, the dynamics of dislocations was addressed in nematic electro-convection [20], but the pinning effects over the underlying stripe pattern considerably altered the interaction law [2].

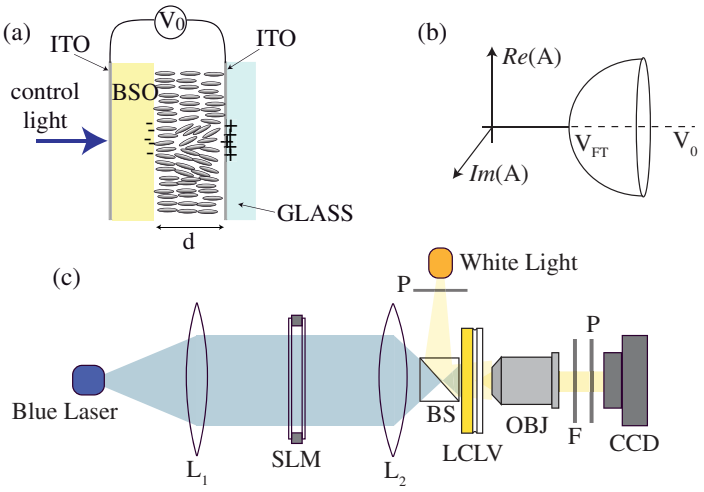

Figure 1. (a) A homeotropic light valve, LCLV; $Bi_{12}SiO_{20}$ (BSO) is used as the photosensitive wall; (b) the degenerate pitchfork bifurcation describing the liquid crystal reorientation; V_{FT} is the Fréedericksz transition voltage and V_0 the applied voltage; (c) the experimental setup: the LCLV is addressed with a control light beam shaped by a spatial light modulator (SLM); the imaging system consists of an objective lens OBJ, a neutral density filter F, crossed polarizers P and a CCD camera for recording.

Subsequent studies of annihilation dynamics of umbilical defects in nematics have shown power law behavior for the vortex pair separation [21], which is compatible with a phenomenological fit based on a constant mobility. However, these observations are in contradiction with the nonlinear mobility theoretically envisaged [3]. In fact, *xy*-models and those stemming from the Frank free energy formalism used for deriving the power law behavior ignore the mobility dependence on speed; the latter gives rise to observable differences at the start of the interaction, with the power law recovered only for large times.

In this paper, we provide the first experimental validation of the logarithmic correction to the vortex speed, demonstrating that nonlinear mobility effects must be taken into account when vortex separations are large, that is, in the early stages of the interaction. These observations lead to a reconciliation of experiments with the theoretical prediction [3]. To investigate the vortex dynamics, we employ nematic liquid crystals (NLCs) in a cell with a photoconductive wall, also known as a liquid crystal light valve (LCLV). The liquid crystals are homeotropically aligned; that is, the nematic director $\vec{n}$ is orthogonal to the confining boundaries, whereas local variations of the voltage across the NLC layer are achieved by a suitable selective illumination of the cell, inducing vortex pairs. The interaction between pairs of oppositely charged vortices—usually called umbilical defects in the context of NLC—is measured and compared against theory in order to determine its governing law(s). The results support the need for a correction introduced by a nonlinear, logarithmic mobility via a phase renormalization [22, 23].

1. The experimental setup

Our setup is sketched in figure 1. As illustrated in figure 1(a), a layer of NLCs (MLC6608 from Merck) was sandwiched between the two parallel interfaces defining an LCLV, i.e.

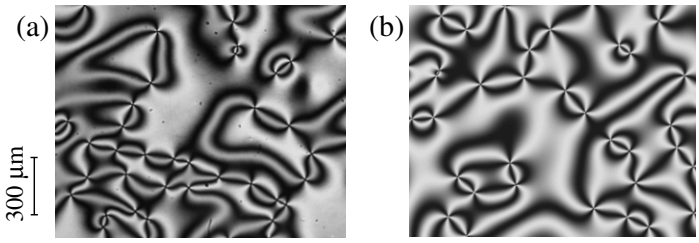

Figure 2. A vortex gas: (a) experimental snapshot recorded under white-light illumination for the cell in between crossed polarizers and for uniform laser illumination of the photosensitive wall; (b) numerical simulations of equation (4) for parameters corresponding to the experimental conditions.

a homeotropic cell of thickness $d = 15\,\mu$m formed by a glass plate and a slab of the transparent photoconductor $Bi_{12}SiO_{20}$ (BSO). The latter was a $25 \times 25\,mm^2$ square crystal of thickness 1 mm. The outer surface of the photoconductor and the inner surface of the glass plate were uniformly coated with thin transparent indium–tin oxide film electrodes in order to apply an external voltage V_0 across the cell. The employed NLC is characterized by a negative dielectric anisotropy, i.e. $\varepsilon_a = \varepsilon_\parallel - \varepsilon_\perp < 0$, with $\varepsilon_\parallel$ and $\varepsilon_\perp$ the dielectric susceptibilities for low-frequency electric fields parallel and orthogonal to the long axis of the NLC molecules, respectively. By means of a suitable surface treatment prior to the cell assembly, the average orientation of the molecules was arranged with their long axes (i.e. director) orthogonal to the confining walls (i.e. homeotropic alignment). When a (low-frequency) bias V_0 is applied to the LCLV, due to the negative ε_a the NLC molecules tend to reorient perpendicularly to the electric field lines; hence, the 2π azimuthal degeneracy around the field direction imposes rotational invariance and the molecules can arbitrarily align in any direction, giving rise to the spontaneous formation of spatial domains separated by point-like defects or vortices [13]. The corresponding degenerate pitchfork bifurcation is illustrated in figure 1(b), where A is the amplitude of the complex field that describes the molecular reorientation.

The light valve allows control of the director tilt both electrically, via the applied voltage V_0, and optically, thanks to photo-induced changes of the BSO conductivity [24]. A laser beam of wavelength $\lambda = 474$ nm was expanded and collimated to a diameter of 1 cm, with an intensity incident on the LCLV of about $3\,mW\,cm^{-2}$. As shown in figure 1(c), before impinging on the LCLV, the beam was amplitude modulated by a computer-controlled spatial light modulator (SLM), the latter essentially consisting of a liquid crystal display (1 inch diagonal size) with a resolution of 1024×768 pixels and an 8-bit intensity dynamics. A lens could image the programmed SLM mask onto the BSO side of the LCLV, allowing the selective illumination of regions where light-induced reorientation could take place and vortices could emerge. Vortices were detected/imaged by placing the LCLV between crossed polarizers and using a CCD camera to record images under white-light illumination. As the bias V_0 was increased beyond the Fréedericskz threshold ($V_{FT} = 3.2$ V in our sample), the NLC molecules started to reorient and vortices abruptly appeared; such a creation process was followed by a coarsening process with the mutual annihilation of vortices with opposite topological charges.

Figure 2(a) displays a typical snapshot acquired just above the Fréedericskz transition ($V_0 = 6$ V rms at 200 Hz): the photoconductor was uniformly illuminated by the laser beam (intensity $2.7\,mW\,cm^{-2}$) and a homogeneous vortex gas was obtained. Each vortex is readily

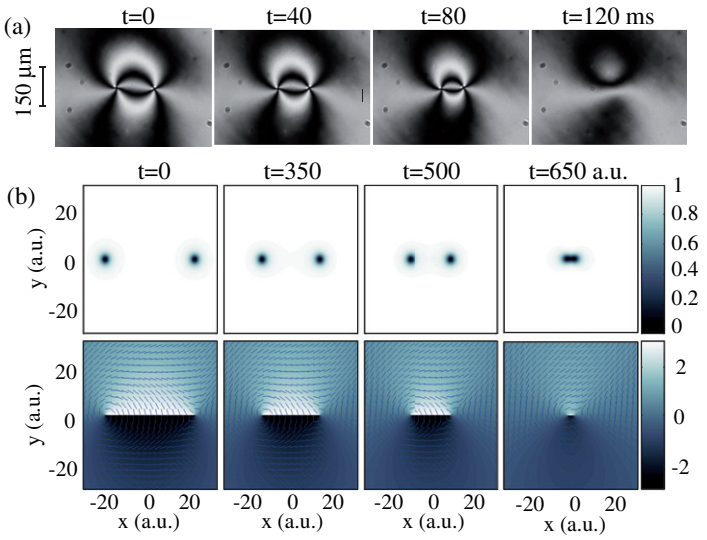

Figure 3. Vortex-pair interaction: (a) experimental snapshots at four successive instant times; (b) numerical simulations; top: intensity field, bottom: phase (gray levels) and nematic director distribution (lines).

identified by the crossing of four black arms, corresponding to a 2π phase shift of the light passing through crossed polarizers; the sign of each charge is determined by rotating one of the polarizers and monitoring the azimuthal motion of the black arms around the defect. Figure 2(b) shows a vortex gas obtained by numerical simulations of the model equation (4) described below. By plotting $[\sin(2\theta)]^2$, where θ is the director tilt, we obtain qualitatively the same picture as the experimental ones. Figure 3(a) shows enlarged images of two neighboring vortices, with their interaction in time illustrated by four successive snapshots. The vortices annihilated before the snapshot in the last panel of figure 3(a). Figure 3(b) shows numerical simulations, with two interacting vortices displayed in four successive instants. Figure 3(b) displays the light intensity (top row), phase and director field (bottom).

2. Theoretical description

In order to describe the vortex nucleation and evolution, we derive a simple model in the vicinity of the Fréedericksz transition, a limit where analytical results are accessible as NLC molecules are weakly tilted from the longitudinal $\hat{z}$-axis and backflow can be neglected. The dynamical equation for the molecular director $\vec{n}$ reads [13, 25]

$$\begin{aligned}\gamma\,\partial_t\vec{n} = {} & K_3[\nabla^2\vec{n} - \vec{n}(\vec{n}\cdot\nabla^2\vec{n})] + (K_3 - K_1)[\vec{n}(\vec{n}\cdot\vec{\nabla})(\vec{\nabla}\cdot\vec{n}) - \vec{\nabla}(\vec{\nabla}\cdot\vec{n})] \\ & + (K_2 - K_3)[2(\vec{n}\cdot\vec{\nabla}\times\vec{n})(\vec{n}(\vec{n}\cdot\vec{\nabla}\times\vec{n}) - \vec{\nabla}\times\vec{n}) + \vec{n}\times\vec{\nabla}(\vec{n}\cdot\vec{\nabla}\times\vec{n})] \\ & + \epsilon_a(\vec{n}\cdot\vec{E})[\vec{E} - \vec{n}(\vec{n}\cdot\vec{E})], \end{aligned} \tag{1}$$

where γ is the rotational viscosity and $\{K_1, K_2, K_3\}$ are the NLC elastic constants. The homeotropic state, $\vec{n} = \hat{z}$, undergoes a stationary instability for critical values of the electric field, $\vec{E} = E\hat{z}$, which match the Fréedericksz threshold

$$|E_{FT}| = \sqrt{-K_3\pi^2/d^2\epsilon_a}. \tag{2}$$

Correspondingly, the NLC layer exhibits a transition for the critical voltage $V_{\mathrm{FT}} = \sqrt{-K_3\pi^2/\epsilon_{\mathrm{a}}}$. Close to the transition point we can introduce the ansatz

$$\vec{n} \approx \begin{pmatrix} u(r_\perp, t)\sin(\pi z/d) \\ w(r_\perp, t)\sin(\pi z/d) \\ 1 - \frac{1}{2}(u^2+w^2)\sin^2(\pi z/d) \end{pmatrix},$$

where z and $r_\perp$ are the longitudinal and transverse coordinates, respectively, and the elastic constants are assumed to be of the same order ($K_1 \sim K_2 \sim K_3$). After straightforward calculations, by using the complex field

$$A(\rho_\perp, t) = (u + \mathrm{i}w)/\sqrt{4d^2\gamma/\pi^2(2K_1 - 3K_3)}, \tag{3}$$

and scaling the space as $r_\perp = \rho_\perp\sqrt{2/(K_1+K_2)}$, we obtain

$$\partial_t A = \mu A - |A|^2 A + \nabla_\perp^2 A, \tag{4}$$

where $\mu \equiv (-\epsilon_{\mathrm{a}}E_{\mathrm{c}}^2 - K_3\pi^2/d^2)/\gamma$, with E_{c} the effective electric field across the NLC layer. The above model admits stable vortex solutions with topological charge ± 1 [2]. Figures 2 and 3 illustrate the observed vortex solutions.

The analysis of the vortex interaction law is complicated because the energy associated with each vortex diverges logarithmically with the size of the system [25]. Thereby, the interaction between distant vortices has an infinite mobility [3]. When considering the role of propagation in the phase equation, we can renormalize the mobility by assuming that the vortices move in a quasi-stationary fashion, i.e. that the phase disturbance one of them undergoes due to the presence of another (or others) shifts infinitesimally; then, again, we can take the phase perturbation in the new vortex position and continuously generate the interaction. This procedure yields the vortex-pair interaction law [3]

$$\dot{r}M(\dot{r}) = v\log\left(\frac{v_0}{v}\right) = \frac{q}{r}, \tag{5}$$

which holds valid for both large and small vortex separation. Here r is the vortex separation, $v \equiv \dot{r}$ its time derivative, q the product of the topological charges ($q = \pm 1$) and v_0 the order of the vortex collision speed. Note that the pair interaction law (5) is not valid when the vortices are merging. The expression $M(\dot{r}) \equiv \log(v_0/v)$ accounts for vortex mobility. At low speed ($v/v_0 \ll 1$), that is, for large vortex separation, the mobility leads to a dynamical correction of the interaction law, whereas at large speed, that is, for small separation, it can be approximated by a constant. In the limit of constant mobility, equation (5) can be integrated, yielding the analytical expression

$$r(t) = r_0\sqrt{1 - t/t_{\mathrm{col}}}, \tag{6}$$

with $t_{\mathrm{col}} = -r_0^2/2q$ the collision time and $r_0 = r(0)$. This provides the phenomenological description for which the interaction law is characterized by a force inversely proportional to the vortex separation.

3. Verification of the vortex-pair interaction law

By employing the SLM, we could selectively create areas above the critical voltage V_{FT}, where we were able to isolate pairs of oppositely charged vortices, as visible in figure 3(a). In order to study their interaction, we removed the polarizer and improved the contrast between

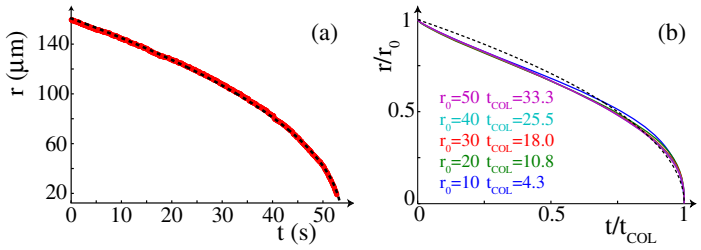

Figure 4. Vortex separation versus time. (a) Measurements: the thick (red) solid line connects the experimental points; the (black) dashed line is a best fit with $r = r_0\sqrt{1 - t/t_{\rm col}}$, $r_0 = 160.7\,\mu$m and $t_{\rm col} = 53.68$ s. (b) Numerical simulations for various r_0, $t_{\rm col}$; the dotted line is the curve $r = r_0\sqrt{1 - t/t_{\rm col}}$.

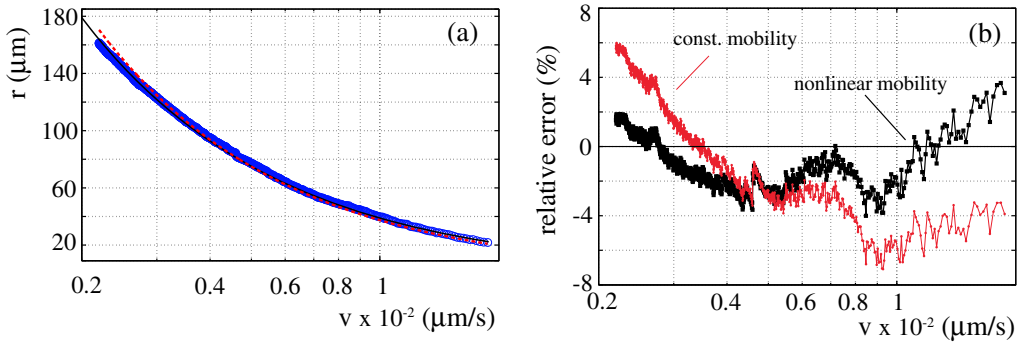

Figure 5. (a) Vortex separation r versus speed v (in the logarithmic scale). Circles: experimental data; the experimental error is contained in their respective radius; dashed (red) line: best fit with constant mobility $rv = q/M_0$, $q/M_0 = 0.3744\,\mu\text{m}^2\,\text{s}^{-1}$; solid (black) line: best fit with nonlinear mobility $rv = q/[M_1\log(v_0/v)]$, $q/M_1 = 7.23\,543\,\mu\text{m}^2\,\text{s}^{-1}$, $v_0 = 1190\,889\,\mu\text{m}\,\text{s}^{-1}$; (b) the corresponding relative error.

illuminating beam and vortex core, the latter appearing as a well contrasted spot over a homogeneous background. Defining a grayscale threshold to identify a vortex, we employed particle-tracker software to locate vortices and their trajectories during their interaction, yielding data on vortex separation versus time, $r(t)$, and speed, $v(t)$. Figure 4(a) plots the measured evolution of $r(t)$. For comparison, figure 4(b) graphs the numerically simulated vortex separation for various initial values r_0 and, correspondingly, different collision times $t_{\rm col}$. The scaling $r(t) \sim t^{1/2}$, predicted for a constant mobility, holds quite well at long times (small separations) but gives rise to appreciable deviations at short times (large separations). Note that in the experimental graph (figure 4(a)) the data are not plotted for separations shorter than 20 μm, because for such distances the vortices nearly coalesce, with their gap becoming comparable to the core size.

In order to emphasize the effect of mobility, figure 5(a) plots vortex separation r versus speed v and compares the data against two interpolating functions, namely for a constant mobility $rv = q/M_0$, $q/M_0 = 0.3744\,\mu\text{m}^2\,\text{s}^{-1}$ and a nonlinear mobility

$$rv = q/[M_1\log(v_0/v)], \tag{7}$$

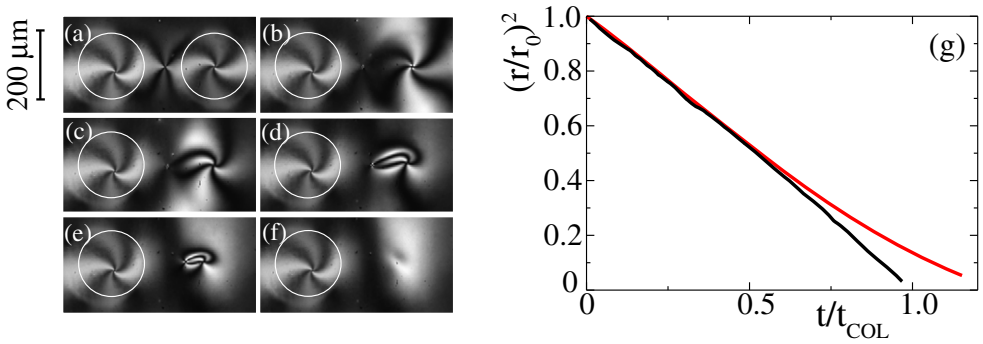

Figure 6. Instantaneous snapshots showing (a) three light-induced vortices; the circles indicate the laser-illuminated regions; (b)–(f) pair interaction; (g) the measured distance versus time (brighter line) and comparison with the measurements without external perturbations (darker line); both curves are normalized to the vortex initial distance r_0 and collision time t_0 of the unperturbed pair.

$q/M_1 = 7.2354\,\mu\mathrm{m}^2\,\mathrm{s}^{-1}$ and $v_0 = 1.1909\,\mathrm{m\,s}^{-1}$, respectively. The best fits are obtained with a least-square procedure. The two fits overlap only at intermediate values of speed; however, both at large and small speeds the effect of a non-constant mobility becomes significant. More precisely, the constant mobility and the nonlinear mobility fits coincide when $v = v_0 \exp(-M_0/M_1)$, which occurs for $v = 0.48 \times 10^{-2}\,\mu\mathrm{m\,s}^{-1}$. Here, v_0 is not a 'physical' speed but represents, instead, the weight of the logarithmic correction. It also takes into account other renormalization phenomena, such as the backflow and the deformation of the vortex core, that are, at first order, neglected in the theory. Figure 5(b) plots the relative error for the case of constant and renormalized mobility, emphasizing the increased accuracy from the latter. The relative error is clearly much larger when using a constant mobility fit than for the nonlinear mobility fit. Precisely, the total (integrated) error power is 4.18 times greater for the constant mobility fit. Note that, while to zero order a constant mobility is a reasonable approximation, consistent with previous observations [3, 19, 20], the role of a logarithmic mobility is fundamental from a theoretical point of view, as it renormalizes the effects of an infinite mobility.

Finally, we checked how the interaction is modified by a third vortex. As illustrated in figure 6(a), three vortices were induced by keeping the voltage V_0 slightly below V_{FT} and illuminating the LCLV with two discs of laser light (intensity $4\,\mathrm{mW\,cm}^{-2}$). A positive vortex is induced inside each disc, while a negative one appears in between, due to the required reconnection of the distorted field lines of the nematic distribution. When one of the disc constraints is released (figure 6(b)), the (negative and positive) free vortices interact (figures 6(c)–(e)) and annihilate (figure 6(f)). Their measured distance $r = r(t)$ versus time is plotted in figure 6(g) and compared with their separation in the absence of external perturbations. In order to emphasize the deviation from the power law behavior, the data for both constrained and unconstrained dynamics were normalized to the collision time for the unperturbed vortex pair. The deviation from the $t^{1/2}$ law is significant, as the presence of the third defect slows down the interaction considerably by introducing screening effects [26].

4. Conclusions

Using NLCs in a light-valve geometry, we experimentally studied vortex-pair interaction. The measurements demonstrate the importance of the propagation of the vortex phase as the latter introduces a weakly nonlinear mobility. The theoretical prediction for a logarithmic dependence of the mobility on the vortex speed results in good agreement with the data, thus reconciling the theory with the experimental observations. The presence of a third vortex substantially lowers the vortex-pair interaction speed. Besides their fundamental relevance, the findings also pinpoint the accuracy of the optical addressing and pave the way for further developments on the management of soft-matter vortices.

Acknowledgments

We acknowledge helpful discussions with T Nagaya. MGC, UB and SR acknowledge financial support from the ANR international program (project number ANR-2010-INTB-402-02 (ANR-CONICYT39)) 'COLORS titled'. MGC acknowledges funding received from FONDECYT project number 1120320. GA acknowledges travel funding received from the Program for Internationalisation at University Roma Tre.

References

[1] Nicolis G and Prigogine I 1977 *Self-Organization in Non Equilibrium Systems* (New York: Wiley)
[2] Pismen L M 2006 *Patterns and Interfaces in Dissipative Dynamics* (Berlin: Springer)
[3] Pismen L M 1999 *Vortices in Nonlinear Fields* (Oxford: Clarendon)
[4] Coullet P, Gil L and Rocca F 1989 *Opt. Commun.* **73** 403
[5] Arecchi F T *et al* 1991 *Phys. Rev. Lett.* **67** 3749
[6] Simpson N B, Allen L and Padgett M J 1996 *J. Mod. Opt.* **43** 2485
[7] Grier D G 2003 *Nature* **424** 810
[8] Arnaut H H and Barbosa G A 2000 *Phys. Rev. Lett.* **85** 286
[9] Tamburini F *et al* 2006 *Phys. Rev. Lett.* **97** 163903
[10] Serabyn E, Mawet D and Burruss R 2010 *Nature* **464** 1018
[11] Marrucci L, Manzo C and Paparo D 2006 *Phys. Rev. Lett.* **96** 163905
[12] Barboza R, Bortolozzo U, Assanto G, Vidal-Henriquez E, Clerc M G and Residori S 2012 *Phys. Rev. Lett.* **109** 143901
[13] de Gennes P G and Prost J 1993 *The Physics of Liquid Crystals* 2nd edn (Oxford: Clarendon)
[14] Frisch T *et al* 1994 *Phys. Rev. Lett.* **72** 1471
[15] Pargellis A N, Green S and Yurke B 1994 *Phys. Rev.* E **49** 4250
[16] Brasselet E and Loussert C 2011 *Opt. Lett.* **36** 719
[17] Lavrentovich O D 2011 *Proc. Natl Acad. Sci. USA* **108** 5143
[18] Smalyukh I I 2011 *Nature* **478** 330
[19] Nagaya T, Hotta H and Orihara H 1991 *J. Phys. Soc. Japan* **60** 1572
[20] Tóth P *et al* 2002 *Europhys. Lett.* **57** 824
[21] Dierking I *et al* 2005 *Phys. Rev.* E **71** 061709
[22] Pismen L M and Rodriguez J D 1990 *Phys. Rev.* A **42** 2471
[23] Rica S and Tirapegui E 1991 *Phys. Lett.* A **161** 53
[24] Aubourg P, Huignard J P, Hareng M and Mullen R A 1982 *Appl. Opt.* **21** 3706
[25] Chandrasekhar S 1992 *Liquid Crystals* (Cambridge: Cambridge University Press)
[26] Serfaty S 2007 *J. Eur. Math. Soc.* **9** 383